



Doppler Rate Estimation for OTFS via Large-Scale Antenna Array

SHAN Yaru¹, WANG Fanggang¹, HAO Yaxing¹,
HUA Jian², XIN Yu²

(1. Beijing Jiaotong University, Beijing 100044, China;
2. ZTE Corporation, Shenzhen 518057, China)

DOI: 10.12142/ZTECOM.202501015

<https://kns.cnki.net/kcms/detail/34.1294.TN.20250103.1627.002.html>,
published online January 6, 2025

Manuscript received: 2024-03-22

Abstract: Orthogonal time frequency space (OTFS) can resist the Doppler effect and guarantee reliable communication in high-speed scenarios. However, the Doppler rate induced by the relative acceleration between the transmitter and receiver degrades the performance of the OTFS. So far, the impact of the Doppler rate on OTFS systems has not been addressed. In this paper, we first introduce the Doppler rate in the OTFS system and derive the delay-Doppler domain input-output relation. In addition, the impact of the Doppler rate on the effective delay-Doppler domain channel is characterized by utilizing the first mean value theorem for definite integrals to avoid complicated integrals. To mitigate the effect of the Doppler rate, a large-scale antenna array is arranged at the receiver to separate each path of the multi-path channel through a high-resolution spatial matched filter beamformer. Next, the Doppler rate estimation scheme for an arbitrary order Doppler rate is proposed based on the successive interference cancellation pattern and the maximization of the spectrum of the ratio of high-order moments between the received samples in the identified branch and the transmitted samples. Finally, the estimation accuracy of the Doppler rate and the error performance of the proposed transceiver are validated by the numerical results.

Keywords: beamforming; Doppler rate; OTFS

Citation (Format 1): SHAN Y R, WANG F G, HAO Y X, et al. Doppler rate estimation for OTFS via large-scale antenna array [J]. *ZTE Communications*, 2025, 23(1): 115 - 122. DOI: 10.12142/ZTECOM.202501015

Citation (Format 2): Y. R. Shan, F. G. Wang, Y. X. Hao, et al., "Doppler rate estimation for OTFS via large-scale antenna array," *ZTE Communications*, vol. 23, no. 1, pp. 115 - 122, Mar. 2025. doi: 10.12142/ZTECOM.202501015.

1 Introduction

Orthogonal time frequency space (OTFS) modulation has been proposed to overcome the high Doppler effect^[1-2]. Specifically, the information-bearing symbols are modulated in the delay-Doppler domain rather than the time-frequency domain of the orthogonal frequency division multiplexing. Each symbol in the delay-Doppler domain is transformed into the whole time-frequency domain by the two-dimensional inverse symplectic finite Fourier transform (ISFFT), which enables the OTFS to harness the full diversity^[3]. The delay-Doppler domain captures the physical characteristics including the delay shifts and the Doppler shifts of the channel, which enables the sparsity of the channel^[4]. The maximum delay and the maximum Doppler shift are within the corresponding range of the delay-Doppler domain.

Therefore, the delay-Doppler domain channel is underspread and quasi-stationary. The sparse and relatively quasi-stationary characteristics in the delay-Doppler domain benefit the channel estimation and the data detection tasks for OTFS.

In mobile radio transmission scenarios, such as the radar detection, low earth orbit (LEO) satellites, and millimeter-wave systems, the received signal may experience significant time-varying Doppler distortion due to the relative motion between the transceivers^[5-8]. Then the Doppler rate as a high-order motion parameter related to the motion acceleration rate must be considered in the system model. Thus, the Doppler shift is no longer a constant but a variable that changes with time. Various methods are adopted to address the Doppler rate under different scenarios. To image a ground-moving target with a synthetic radar system, the third-order Doppler frequency mitigation schemes are designed. The coherent integration detection schemes based on the Keystone transform and even the second-order Keystone transform, and the generalized Hough-high-order ambiguity function are proposed in Refs. [5] and [6], respectively. In Ref. [7], a new fast Doppler shift and Doppler rate joint acquisition method derived from the spectrum method is proposed for hypersonic vehicle communications. Based on the sequential importance sampling,

This work was supported in part by the Fundamental Research Funds for the Central Universities under Grant No. 2022JBQY004, the National Natural Science Foundation of China under Grant Nos. 62471026 and 62221001, the Zhongguancun Xinxu Disruptive Technology Innovation Foundation under Grant No. ZZ-2024-001, the Joint Funds for Railway Fundamental Research of National Natural Science Foundation of China under Grant No. U2368201, the Postdoctoral Fellowship Program and China Postdoctoral Science Foundation BX20240471, and ZTE Industry-University-Institute Cooperation Funds under Grant No. HC-CN-03-2019-12.

the joint estimation of the carrier phase, Doppler shift, Doppler rate, and data detection using particle filters is proposed in Ref. [8]. However, the above-mentioned schemes only consider the Doppler rate in the scenario where only a single path exists and is not always valid in the common communication systems. Moreover, to the best of our knowledge, there does not exist any open literature that introduces and then addresses the Doppler rate effect for OTFS.

In this paper, we first introduce the Doppler rate in the OTFS system. The delay-Doppler domain input-output relation is derived under an arbitrary-order Doppler rate. In addition, the Doppler rate effect is characterized by taking advantage of the first mean value theorem for definite integrals. Then, the system model is proposed by arranging a large-scale antenna array at the receiver and a joint frame structure is considered, where the first transmission frame is utilized to estimate the Doppler rate and then the Doppler rate is compensated in the subsequent frames through precoding. Next, the Doppler rate estimation and compensation scheme that applies to the system with an arbitrary-order Doppler rate and performs in the first frame is proposed. Although some studies utilize the angle domain to separate scattering paths, the existing literature does not account for the Doppler rate effect^[9]. The main contributions of this paper are summarized as follows:

1) The Doppler rate is first introduced in the OTFS system. Based on the introduction of the effect of the Doppler rate, the delay-Doppler domain input-output relation is rederived and the influence of the Doppler rate is characterized by utilizing the first mean value theorem for definite integrals.

2) The receiver scheme is designed with a large-scale antenna array to estimate the Doppler rate in each identified branch. Specifically, the different scattering paths are separated in the angle domain to create the signal path condition to simplify the Doppler rate estimation.

3) The Doppler rate mitigation scheme applied to the arbitrary order Doppler rate is proposed by utilizing the maximization of the spectrum of the ratio of high-order moments between the received samples in the identified branch and the transmitted samples.

The remainder of the paper is organized as follows. Section 2 introduces the system model. Section 3 introduces the OTFS transceiver, followed by the Doppler rate estimation in Section 4. The simulation results and conclusions are provided in Sections 5 and 6, respectively.

2 System Model

We first introduce the Doppler rate effect to the delay-Doppler domain channel. Then, the generalized delay-Doppler domain input-output relation for an OTFS system with the arbitrary-order Doppler rate is derived. Finally, the effect of

the Doppler rate is characterized.

2.1 Channel with Doppler Rate*

The delay-Doppler domain channel with the Doppler rate is sparse and is expressed as:

$$h(\tau, \nu, t) = \sum_{p=0}^{P-1} \beta_p \delta(\tau - \tau_p) \delta(\nu - \nu_p - \sum_{q=1}^Q a_q t^q) \quad (1),$$

where P is the total number of the channel taps; β_p and τ_p are the channel coefficient and the delay shift of the p -th path, respectively; $\nu_p = f_d \cos \theta_p$ where f_d is the maximum Doppler shift and θ_p is the angle of arrival of the p -th path; Q is the highest order of the Doppler rate and a_q is the coefficient of the q -th order Doppler rate. The variation of the delay can exist in the high-speed scenarios as in Ref. [10].

2.2 Input-Output Relation in Delay-Doppler Domain

Without the noise, the delay-Doppler domain input-output relation can be expressed as:

$$y[k, l] = \frac{1}{MN} \sum_{k'=0}^{N-1} \sum_{l'=0}^{M-1} x[k', l'] h_{k,l}[k', l'], \quad k \in \mathcal{I}_N, l \in \mathcal{I}_M \quad (2),$$

where $x[k', l']$ and $y[k, l]$ are the information-bearing symbols and the received symbols in the delay-Doppler domain, respectively; N and M are the numbers of the samples in the Doppler and the delay domain, respectively; $\mathcal{I}_N = [0, 1, \dots, N-1]$ is defined as shorthand hereafter to represent an index set; $h_{k,l}[k', l']$ is the sampled effective delay-Doppler domain channel and can be expressed as:

$$h_{k,l}[k', l'] = \underbrace{\sum_{n=0}^{N-1} \sum_{m=0}^{M-1} \sum_{m'=0}^{M-1} H_{n,m}[n, m'] e^{-j2\pi n(\frac{k-k'}{N})} e^{j2\pi \frac{ml-m'l'}{M}}}_{\triangleq h_{k,l}^{(1)}[k', l']} + \underbrace{\sum_{n=1}^{N-1} \sum_{m=0}^{M-1} \sum_{m'=0}^{M-1} H_{n,m}[n-1, m'] e^{-j2\pi(\frac{nk}{N} - \frac{(n-1)k'}{N})} e^{j2\pi \frac{ml-m'l'}{M}}}_{\triangleq h_{k,l}^{(2)}[k', l']} \quad (3).$$

We denote $H_{n,m}[n', m']$ as the sampled time-frequency domain effective channel. With the rectangular pulses considered for the transmit and the receive pulse-shaping functions, $H_{n,m}[n', m']$ is nonzero when $n' = n$ or $n' = n-1$, and $H_{n,m}[n, m']$ and $H_{n,m}[n-1, m']$ are expressed as:

$$H_{n,m}[n, m'] = \sum_{p=0}^{P-1} \frac{\beta_p}{T} \int_0^{T-\tau_p} e^{j2\pi\left(\nu_p + \sum_{q=1}^Q a_q (t' + \tau_p + nT)^q\right)(t' + nT)} \times e^{j2\pi m' \Delta f t''} e^{-j2\pi m \Delta f (t' + \tau_p)} dt'' \quad (4),$$

* We pay attention to the time-varying Doppler shift in this manuscript and the effect of the time-varying delay will be addressed in our future work.

$$H_{n,m}[n-1,m'] = \sum_{p=0}^{P-1} \frac{\beta_p}{T} \int_{T-\tau_p}^T e^{j2\pi \left(\nu_p + \sum_{q=1}^Q a_q (l'' + \tau_p + (n-1)T)^q \right) (l'' + (n-1)T)} \times e^{j2\pi m' \Delta f l''} e^{-j2\pi m \Delta f (l'' + \tau_p)} dl'' \quad (5)$$

We can see from Eqs. (3) – (5) that the calculation of the $h_{k,l}[k',l']$ involves the integral of the function with the form $\int_{a_1}^{b_1} e^{j\pi \nu l} dl$, which is difficult to calculate directly.

2.3 Doppler Rate Effect Characterization

To demonstrate the influence of the Doppler rate, the first mean value theorem for definite integrals is utilized to avoid the complicated calculation in Eqs. (4) and (5). We assume that $\exists \xi_1 \in [0, T - \tau_p]$ and $\exists \xi_2 \in [T - \tau_p, T]$, and Eqs. (6) and (7) hold.

From Eq. (3), we can further express $h_{k,l}^{(1)}[k',l']$ and $h_{k,l}^{(2)}[k',l']$ as:

$$H_{n,m}[n,m'] = \sum_{p=0}^{P-1} \frac{\beta_p (T - \tau_p)}{T} e^{j2\pi m' \Delta f \xi_1} e^{-j2\pi m \Delta f (\xi_1 + \tau_p)} \times e^{j2\pi \left(\nu_p + \sum_{q=1}^Q a_q (\xi_1 + \tau_p + nT)^q \right) (\xi_1 + nT)} \quad (6)$$

$$H_{n,m}[n-1,m'] = \sum_{p=0}^{P-1} \frac{\beta_p \tau_p}{T} e^{j2\pi m' \Delta f \xi_2} e^{-j2\pi m \Delta f (\xi_2 + \tau_p)} \times e^{j2\pi \left(\nu_p + \sum_{q=1}^Q a_q (\xi_2 + \tau_p + (n-1)T)^q \right) (\xi_2 + (n-1)T)} \quad (7)$$

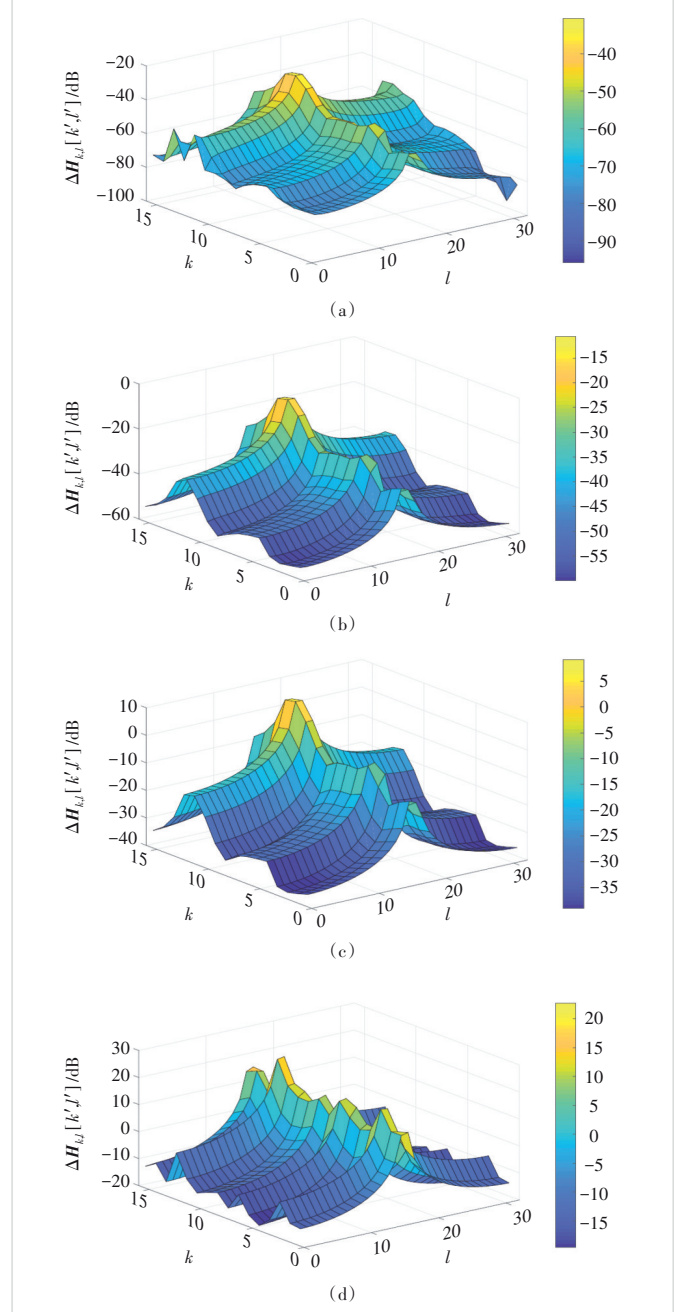
$$h_{k,l}^{(1)}[k',l'] = \sum_{p=0}^{P-1} \frac{\beta_p}{T} (T - \tau_p) e^{j2\pi \nu_p \xi_1} \frac{e^{j2\pi M (\Delta f \xi_1 - \frac{l'}{M})} - 1}{e^{j2\pi (\Delta f \xi_1 - \frac{l'}{M})} - 1} \frac{e^{-j2\pi M (\Delta f (\xi_1 + \tau_p) - \frac{l}{M})} - 1}{e^{-j2\pi (\Delta f (\xi_1 + \tau_p) - \frac{l}{M})} - 1} \times \sum_{n=0}^{N-1} e^{j2\pi \left(\sum_{q=1}^Q a_q (\xi_1 + \tau_p + nT)^q \right) (\xi_1 + nT) + \nu_p n T - n \frac{k-k'}{N}} \quad (8)$$

$$h_{k,l}^{(2)}[k',l'] = \sum_{p=0}^{P-1} \frac{\beta_p \tau_p}{T} e^{j2\pi \nu_p \xi_2} \frac{e^{j2\pi M (\Delta f \xi_2 - \frac{l'}{M})} - 1}{e^{j2\pi (\Delta f \xi_2 - \frac{l'}{M})} - 1} \times \frac{e^{-j2\pi M (\Delta f (\xi_2 + \tau_p) - \frac{l}{M})} - 1}{e^{-j2\pi (\Delta f (\xi_2 + \tau_p) - \frac{l}{M})} - 1} \times \sum_{n=1}^{N-1} e^{j2\pi \left(\sum_{q=1}^Q a_q (\xi_2 + \tau_p + (n-1)T)^q \right) (\xi_2 + (n-1)T) + \nu_p (n-1)T - \frac{nk}{N} + \frac{(n-1)k'}{N}} \quad (9)$$

For an explicit illustration of the Doppler rate effect, we mesh

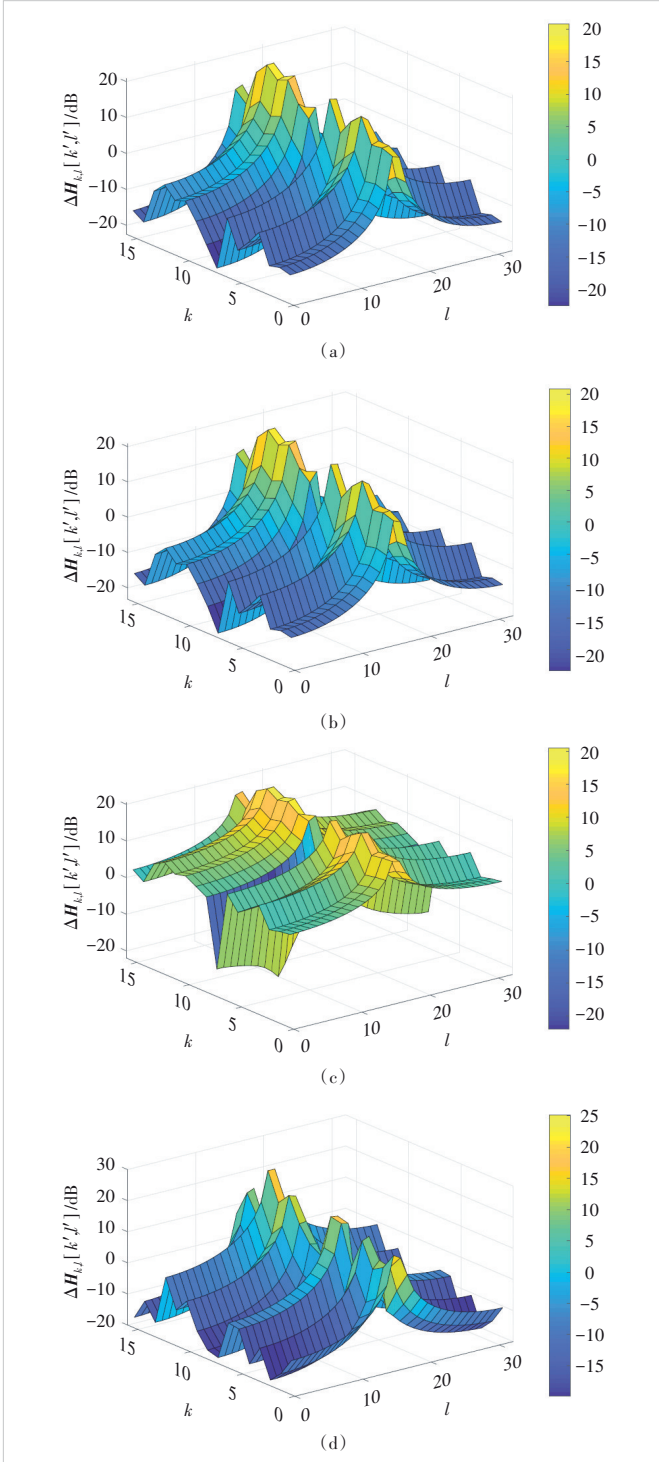
the difference of the delay-Doppler domain channel $\Delta H_{k,l}[k',l'] = |h_{k,l}[k',l'] - \hat{h}_{k,l}[k',l']|^2$, given the fixed $k' = \frac{N}{2}$ and $l' = \frac{M}{2}$, where $\hat{h}_{k,l}[k',l']$ is the delay-Doppler domain channel without the Doppler rate influence, i.e., $a_q = 0, \forall q$. The values of N and M are set as 16 and 32, respectively. As the different values of ξ_1 and ξ_2 would have little impact on the characterization of the channel, we set $\xi_1 = \frac{T - \tau_{\max}}{2}, \xi_2 = \frac{2T - \tau_{\max}}{2}$.

The highest orders of the Doppler rate in Figs. 1 and 2 are 1



▲ Figure 1. Difference of the delay-Doppler domain channel matrix $\Delta H_{k,l}[k',l']$ meshes with the highest order of the Doppler rate $Q=1$, where the values of the a_1 in (a), (b), (c), and (d) are set as 49 Hz/s, 490 Hz/s, 4900 Hz/s, and 49×10^8 Hz/s, respectively

and 2, respectively. We can see that the difference of the delay-Doppler domain channel becomes larger as the values of the Doppler rate increase. Compared with Fig. 1, we can see that



▲ Figure 2. Difference of the delay-Doppler domain channel matrix $\Delta H_{k,l}[k',l']$ meshes with the highest order of the Doppler rate $Q=2$, where the values of a_2 are all set as 49×10^8 Hz/s²; the values of a_1 in (a), (b), (c), and (d) are set as 49 Hz/s, 490 Hz/s, 4 900 Hz/s, and 49×10^8 Hz/s, respectively

the variance of the delay-Doppler domain channel is more sophisticated under a higher order of the Doppler rate in Fig. 2. Therefore, it is necessary to design a scheme to estimate and then compensate the effect of the Doppler rate to guarantee reliable communication in high-speed scenarios.

3 Receiver Design

The joint frame structure is designed, where the time-domain linear frequency modulated signal is sent in the first frame to estimate the Doppler rate and then the Doppler rate compensation is performed in the subsequent frames by using the Doppler rate estimate in the first frame.

The diagram of the proposed scheme in the first frame is demonstrated in Fig. 3. We consider a downlink high-mobility transmission scenario where a large-scale antenna array is arranged at the receiver. In addition, the value of the arbitrary order of the Doppler rate is assumed as a constant in the system model. The multi-path channel from the base station to the b -th antenna is expressed as:

$$h_b(t, \tau) = \sum_{p=0}^{P-1} \beta_p e^{j \left(2\pi \left(\nu_p + \sum_{q=1}^Q a_q t^q \right) t + \phi_b \cos \theta_p \right)} \delta(\tau - \tau_p) \quad (10)$$

where $b \in \mathcal{I}_B$, and B is the number of the receive antennas. The phase of the b -th antenna is expressed as:

$$\phi_b = \frac{1}{\lambda} 2\pi b \eta, \quad b \in \mathcal{I}_B \quad (11)$$

where λ is the carrier wavelength; $\eta < 0.5\lambda$ is the antenna distance of the uniform linear array (ULA) and is designed to produce only one beam in each receiving beamformer.

The received signal of the b -th antenna is expressed as:

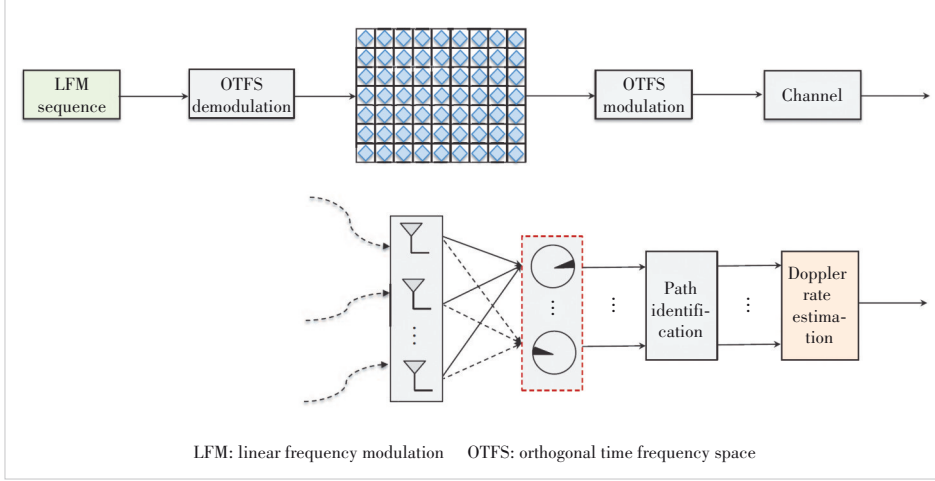
$$r_b(t) = \sum_{p=0}^{P-1} \beta_p e^{j \left(2\pi \left(f_p \cos \theta_p + \sum_{q=1}^Q a_q t^q \right) t + \phi_b \cos \theta_p \right)} s(t - \tau_p) + \tilde{z}_b(t) \quad (12)$$

where $\tilde{z}_b(t)$ is the time domain circularly symmetric complex Gaussian (CSCG) noise of the b -th antenna and it follows $\mathcal{CN}(0, \sigma^2)$ at a time instant.

To separate the multi-path effect, the receive beamforming is implemented by a spatial matched filter. The corresponding steering vector of the b -th antenna is designed as follows.

$$\omega_b(\theta) = e^{j\phi_b \cos \theta}, \quad b \in \mathcal{I}_B \quad (13)$$

After scanning all possible angles, only U branches receive the desired signal. We assume the interested angles are in the set $\Phi = \{\varphi_u | u \in \mathcal{I}_U\}$. In addition, the one-to-one mapping function is defined as $u = \varpi(p)$, $u \in \mathcal{I}_U$, where the index p maps to the identified path u . Therefore, the received signal from the angle φ_u is represented by:


Figure 3. Diagram of the proposed scheme to estimate the Doppler rate in the first frame

$$\begin{aligned}
 r_u(t) &= \frac{1}{B} \sum_{b=0}^{B-1} \omega_b^*(\varphi_u) r_b(t) = \\
 &\beta_p e^{j2\pi \left(f_d \cos \theta_p + \sum_{q=1}^Q a_q t^q \right) t} s(t - \tau_p) + z_u(t) + \\
 &\frac{1}{B} \sum_{b=0}^{B-1} \sum_{\varpi(p') \neq u} \beta_{p'} e^{j2\pi \left(f_d \cos \theta_{p'} + \sum_{q=1}^Q a_q t^q \right) t} \times e^{j\phi_b(\cos \theta_{p'} - \cos \varphi_u)} \quad (14),
 \end{aligned}$$

where

$$z_u(t) = \frac{1}{B} \sum_{b=0}^{B-1} \omega_b^*(\varphi_u) \tilde{z}_b(t), \quad u \in \mathcal{I}_U \quad (15).$$

With the arrangement of a large-scale antenna array, the interference of the identified branch can be ignored and was also proved in our previous work^[11]. Then the received signal of the u -th identified branch can be expressed as:

$$r_u(t) \approx \beta_u e^{j2\pi \left(\nu_u + \sum_{q=1}^Q a_q t^q \right) t} s(t - \tau_u) + z_u(t) \quad (16),$$

where $\beta_u = \beta_p$, $\tau_u = \tau_p$, $\nu_u = f_d \cos \varphi_u$, and $u = \varpi(p)$ is the Doppler shift of the u -th identified branch.

4 Doppler Rate Estimation

In this section, the proposed Doppler rate estimation scheme is introduced to the system with the first-order and the second-order Doppler rate. Then the generalized Doppler rate estimation scheme that applies to the system with an arbitrary-order Doppler rate is illustrated. Finally, the Doppler rate mitigation scheme through precoding is demonstrated.

4.1 First-Order Doppler Rate

For the system only with the first-order Doppler rate, i.e., $Q = 1$, the received samples of the u -th identified branch can be represented by:

$$r_u(n) = \beta_u e^{j2\pi \left(\frac{k_u}{MN} n + \frac{a_1}{(M\Delta f)^2} n^2 \right)} s(n - l_u) \quad (17),$$

where $k_u = \nu_u NT \in \mathbb{R}$ and $l_u = \lfloor \tau_u M\Delta f + 0.5 \rfloor$. After the ISFFT and the Heisenberg transform, the time domain linear frequency modulated sequence $s(n)$ is sent with the length $N_0 = MN - 1$. The estimation of the Doppler rate conducts as follows.

1) Calculate the instantaneous auto-correlation of the $r_u^*(n)$:

$$\begin{aligned}
 A_r(n) &= r_u^*(n) r_u(n + \eta_0) = \\
 &|\beta_u|^2 e^{j2\pi \left(\frac{k_u}{MN} \eta_0 + \frac{a_1}{(M\Delta f)^2} (d_0^2 + 2\eta_0 n) \right)} \quad (18),
 \end{aligned}$$

where $\eta_0 \in (0, N_0)$ is a constant, $n \in [-M_0, M_0 - \eta_0]$, and $M_0 = (N_0 - 1)/2$.

2) Calculate the fourth-order moment $F_r(\eta_1)$:

$$F_r(\eta_1) = \sum_{n=N_1}^{N_2} A_r^*(n) A_r(n + \eta_1) = |\beta_u|^4 e^{j2\pi \frac{2a_1 \eta_0 \eta_1}{(M\Delta f)^2}} \quad (19),$$

where $\eta_1 \in [-(N_0 - \eta_0 - 1), N_0 - \eta_0 - 1]$, $N_1 = \max \{-M_0, -M_0 - \eta_1\}$, and $N_2 = \min \{M_0 - \eta_0, M_0 - \eta_0 - \eta_1\}$.

3) Calculate the forth-order moment of $s(n)$ to obtain $F_s(\eta_1)$. The calculation of the forth-order moment of $s(n)$ follows Eq. (19).

4) Calculate the ratio between $F_r(\eta_1)$ and $F_s(\eta_1)$:

$$\xi(\eta_1) = \begin{cases} \frac{F_r(\eta_1)}{F_s(\eta_1)}, & F_s(\eta_1) \neq 0 \text{ and } \eta_1 \neq 0 \\ \frac{\xi(\eta_1 - 1) + \xi(\eta_1 + 1)}{2}, & \text{otherwise} \end{cases} \quad (20).$$

5) Perform fast Fourier transform on $\xi(\eta_1)$:

$$\begin{aligned}
 \Xi(\bar{l}) &= \sum_{\eta_1 = -(N_0 - \eta_0 - 1)}^{N_0 - \eta_0 - 1} \xi(\eta_1) e^{-j \frac{2\pi \eta_1 \bar{l}}{2(N_0 - \eta_0) - 1}}, \\
 \bar{l} &\in [-(N_0 - \eta_0 - 1), (N_0 - \eta_0 - 1)] \quad (21).
 \end{aligned}$$

6) Maximize $\Xi(\bar{l})$. Find the value of \bar{l} that maximizes $\Xi(\bar{l})$ and then estimate the first-order Doppler rate a_1 as:

$$\hat{a}_1 = \frac{(M\Delta f)^2}{2\eta_0(2N_0 - 2\eta_0 - 1)} \operatorname{argmax}_{\bar{l}} |\Xi(\bar{l})| \quad (22).$$

4.2 Second-Order Doppler Rate

For the system with the second-order Doppler rate, i.e. $Q = 2$,

the received samples can be represented by

$$r_u(n) = \beta_u e^{j2\pi \left(\frac{k}{MN}n + \frac{a_1}{(M\Delta f)^2}n^2 + \frac{a_2}{(M\Delta f)^3}n^3 \right)} s(n - l_u) \quad (23).$$

To cancel the influence of Doppler rates, the designed scheme first estimates the second-order Doppler rate. Then, the effect of the second-order Doppler rate is removed from the received samples. Next, the first-order Doppler rate is estimated and then removed. Based on the estimation of the first-order Doppler rate, the second-order Doppler rate is calculated as follows.

1) Calculate the eighth-order moment $E_r(\eta_2)$:

$$E_r(\eta_2) = F_r(\eta_1)F_r^*(\eta_1 + \eta_2) = |\beta_u|^8 e^{j2\pi \frac{6a_2\eta_0\eta_1\eta_2}{(M\Delta f)^3}} \quad (24),$$

where $\eta_2 \in [-(N_0 - \eta_0 - \eta_1 - 1), N_0 - \eta_0 - \eta_1 - 1]$.

2) Calculate the eighth-order moment $E_s(\eta_2)$. The calculation of the eighth-order moment of $s(n)$ follows Eq. (27).

3) Calculate the ratio between $E_r(\eta_2)$ and $E_s(\eta_2)$:

$$\xi(\eta_2) = \begin{cases} \frac{E_r(\eta_2)}{E_s(\eta_2)}, & E_s(\eta_1) \neq 0 \text{ and } \eta_2 \neq 0 \\ \frac{\xi(\eta_2 - 1) + \xi(\eta_2 + 1)}{2}, & \text{otherwise} \end{cases} \quad (25).$$

4) Perform the fast Fourier transform on $\xi(\eta_2)$:

$$\Xi(\tilde{l}) = \sum_{\eta_2 = -(N_0 - \eta_0 - \eta_1 - 1)}^{N_0 - \eta_0 - \eta_1 - 1} \xi(\eta_2) e^{-j \frac{2\pi\eta_2\tilde{l}}{2(N_0 - \eta_0 - \eta_1 - 1)}}, \quad \tilde{l} \in [-(N_0 - \eta_0 - \eta_1 - 1), (N_0 - \eta_0 - \eta_1 - 1)] \quad (26).$$

5) Maximize $|\Xi(\tilde{l})|$. Find the value of \tilde{l} that maximizes $|\Xi(\tilde{l})|$ and then estimate the second-order Doppler rate a_2 as:

$$\hat{a}_2 = \frac{(M\Delta f)^3}{6\eta_0\eta_1(2N_0 - 2\eta_0 - 2\eta_1 - 1)} \underset{i}{\operatorname{argmax}} |\Xi(\tilde{l})| \quad (27).$$

4.3 Extension to Higher-Order Doppler Rate

We can extend the proposed Doppler rate estimation scheme to a system with an arbitrary-order Doppler rate. For a system with Q -th order Doppler rate, the received samples can be expressed as:

$$r_u(n) = \beta_u e^{j2\pi \left(\frac{k}{MN}n + \sum_{q=1}^Q a_q \left(\frac{n}{M\Delta f} \right)^{q+1} \right)} s(n - l_u) \quad (28).$$

The estimation of the Doppler rate is conducted with a successive interference pattern as follows. The 2^{Q+1} -order moment of the received samples is calculated first. Then the ratio between the 2^{Q+1} -order moment of the received samples and the 2^{Q+1} -order moment of the sent samples is calculated. Next, the fast Fourier transform is utilized to transform the ratio into the fre-

quency domain and obtain the spectrum of the moment. Finally, the spectrum is maximized and the corresponding estimation of the Q -th order Doppler rate a_Q is calculated. Once the Q -th order Doppler rate is estimated, it is removed from the received samples, and the $(Q - 1)$ -th order Doppler rate is calculated and then cancelled. The estimation and the compensation processes continue until the first-order Doppler rate is mitigated. The proposed Doppler rate scheme is unbiased, which can be proved based on the fact that the noise is zero mean CSCG and the Fourier transform does not change the mean value.

4.4 Precoding Scheme

For the frames that transmit the information-bearing symbols, precoding is performed in the delay-Doppler domain to mitigate the effect of the Doppler rate.

From Ref. [4], the time-domain transmitted symbol vector \mathbf{s} can be expressed as:

$$\mathbf{s} = (\mathbf{F}_N^H \otimes \mathbf{I}_M) \mathbf{x}_D \quad (29),$$

where \mathbf{x}_D is the delay-Doppler domain transmit vector and the operation \otimes denotes the Kronecker product. To mitigate the effect of the Doppler rate, time-domain precoding is carried out as:

$$\mathbf{P}\mathbf{s} = \mathbf{P}(\mathbf{F}_N^H \otimes \mathbf{I}_M) \mathbf{x}_D \quad (30),$$

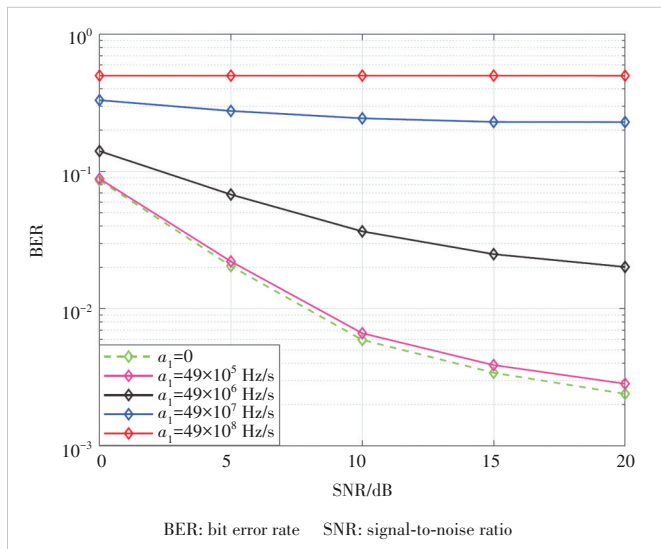
where $\mathbf{P} = \operatorname{diag}\{\mathbf{p}\}$ and the n -th element of the vector is $p_n = e^{-j2\pi \left(\sum_{q=1}^Q \hat{a}_q \left(\frac{n}{M\Delta f} \right)^{q+1} \right)}$, $n \in \mathcal{I}_{MN}$. Since the information-bearing symbols are transmitted in the delay-Doppler domain, the precoding matrix is designed in the delay-Doppler domain as $\mathbf{P}(\mathbf{F}_N^H \otimes \mathbf{I}_M)$.

5 Simulation Results

In this section, we evaluate the performance from the normalized mean squared error (NMSE) of the Doppler rate estimation and the bit error rate (BER) of the proposed scheme. The NMSE of the q -th order Doppler rate is defined as $10 \log_{10}(|a_q - \hat{a}_q|^2/a_q^2)$. We set $N = 32$, $M = 64$, $\Delta f = 150$ kHz, the moving speed $v = 1$ Ma, the carrier frequency $f_c = 4$ GHz, and the modulation scheme is 4 Quadrature Amplitude Modulation (QAM). The delay indices of the channel is $[0, 1, 2, 3, 4, 5]$ and the power of each tap is uniformly distributed. The Doppler shift of the channel is generated by $f_d \cos \theta_p$ where the angle of arrival (AoA) of each path θ_p is independently uniformly distributed in $[0, 2\pi)$. Furthermore, the channel response of all the antenna elements are normalized as 1. Moreover, the receive beamforming is designed with an interval of one degree. For the error performance, the channel estimation in Ref. [11] and the data detection scheme in Ref. [12] are adopted. The value of the Doppler rate is set as large as possible and such setting is suitable especially under the take-off and the landing process of high-speed aircrafts.

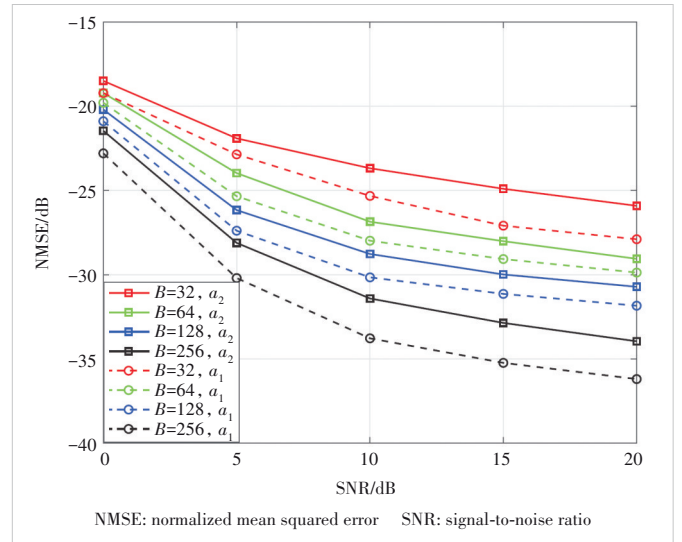
In Fig. 4, we demonstrate the error performance by introducing the different values of the Doppler rate. In addition, the BER is evaluated without the estimation and compensation of the Doppler rate. We can obtain that the error performance when $a_1 \leq 49 \times 10^5$ Hz/s is nearly the same as that without the introduction of the Doppler rate. However, the error performance deteriorates sharply when $a_1 \geq 49 \times 10^5$ Hz/s. Especially, the system cannot even normally work when $a_1 = 49 \times 10^8$ Hz/s. The reason can be explained by comparing the maximum Doppler shift of one OTFS frame Δf and the Doppler shift increment from the Doppler rate $\Delta D = a_1 NT$. When $a_1 = 49 \times 10^5$ Hz/s, the increment of the Doppler shift is $\Delta D = \frac{49 \times 10^5 \times 32}{150 \times 10^3} \approx 1045$ Hz $< 15 \times 10^3$ Hz = Δf . Though without the estimation and the compensation of the Doppler rate, the effect of the Doppler rate can be mitigated in the channel estimation. Thus, the error performance can keep the same as that without the Doppler rate. However, the increment of the Doppler shift can arrive at the value $\Delta D = \frac{49 \times 10^6 \times 32}{150 \times 10^3} \approx 1045$ kHz $> \Delta f$. The Doppler rate cannot be mitigated from the channel estimation deteriorating the error performance. Therefore, the estimation and the compensation of the Doppler rate are necessary to guarantee the reliable communication under such setting.

In Fig. 5, we evaluate the Doppler rate estimation accuracy under $Q = 2$, $a_2 = 49 \times 10^{12}$ Hz/s², and $a_1 = 49 \times 10^8$ Hz/s. We can see that the estimation accuracy of both the second order Doppler rate and the first order Doppler rate improves with the increasing number of the receive antennas. In addition, the estimation accuracy of the first order Doppler rate under $Q = 1$ outperforms that under $Q = 2$. This phenomenon is caused by the proposed successive interference cancellation pattern for the high order Doppler rate.

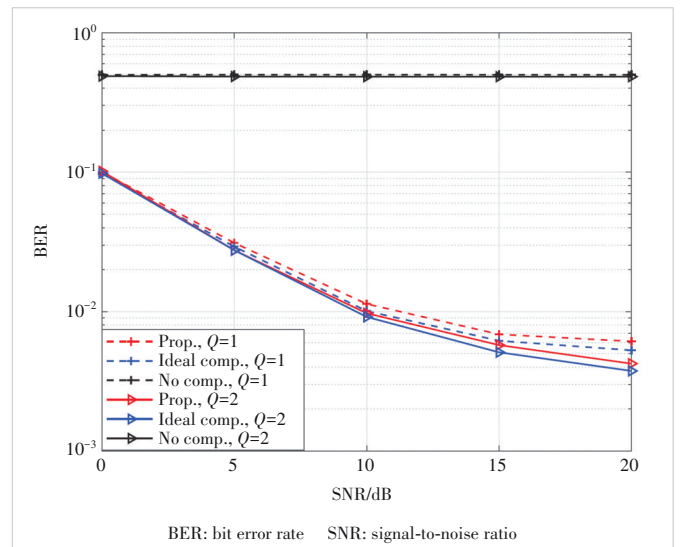


▲ Figure 4. BER is evaluated under the different values of the Doppler rate and without the Doppler rate effect compensation, where the results demonstrate that the error performance deteriorates as the Doppler rate increases

In Fig. 6, we demonstrate the error performance of the proposed transceiver under $Q = 1$ and $Q = 2$. In addition, $\eta_0 = 400$ and $a_1 = 49 \times 10^8$ Hz/s for $Q = 1$; $\eta_0 = 800$, $\eta_1 = 400$, $a_2 = 49 \times 10^{12}$ Hz/s², and $a_1 = 49 \times 10^8$ Hz/s for $Q = 2$. We can see that the proposed transceiver can achieve the same error performance as that with the perfect Doppler rate compensation, indicating the proposed transceiver can effectively mitigate the Doppler rate effect. In addition, the system cannot even normally work without compensating the Doppler rate, which il-



▲ Figure 5. NMSE of the Doppler rate is evaluated under the four values of the receive antenna, namely 32, 64, 128, and 256. The highest order of the Doppler rate is 2, i.e., $Q = 2$, $a_1 = 49 \times 10^8$ Hz/s and $a_2 = 49 \times 10^{12}$ Hz/s². We can see that the performance of the proposed transceiver improves with the increasing number of the receive antenna



▲ Figure 6. BER is evaluated under the three schemes and the two values of the highest order of the Doppler rate. We can see that the proposed scheme can achieve nearly the same performance as the perfect Doppler rate compensation under both the first order and the second order Doppler rate conditions

illustrates the significance of estimating the Doppler rate effect.

6 Conclusions

In this paper, we first introduce the effect of the Doppler rate in the OTFS system and derive the delay-Doppler domain input-output relation. Then the Doppler rate effect is characterized by utilizing the first mean value theorem for definite integrals to avoid the complicated integrals. Aiming at mitigating the Doppler rate effect, the joint frame transceiver scheme, where the Doppler rate is estimated in the first frame and then the effect is removed in the subsequent data frames, is designed by arranging a large-scale antenna array at the receiver. Simulation results demonstrate the efficiency of the proposed scheme.

References

- [1] HADANI R, RAKIB S, TSATSANIS M, et al. Orthogonal time frequency space modulation [C]//IEEE Wireless Communications and Networking Conference (WCNC). IEEE, 2017: 1 - 6. DOI: 10.1109/WCNC.2017.7925924
- [2] HADANI R, MONK A. OTFS: a new generation of modulation addressing the challenges of 5G [EB/OL]. (2018-02-17) [2023-06-15]. <http://arxiv.org/abs/1802.02623>
- [3] SURABHI G D, AUGUSTINE R M, CHOCKALINGAM A. On the diversity of uncoded OTFS modulation in doubly-dispersive channels [J]. IEEE transactions on wireless communications, 2019, 18(6): 3049 - 3063. DOI: 10.1109/TWC.2019.2909205
- [4] RAVITEJA P, HONG Y, VITERBO E, et al. Practical pulse-shaping waveforms for reduced-cyclic-prefix OTFS [J]. IEEE transactions on vehicular technology, 2019, 68(1): 957 - 961. DOI: 10.1109/TVT.2018.2878891
- [5] HUANG P H, LIAO G S, YANG Z W, et al. Long-time coherent integration for weak maneuvering target detection and high-order motion parameter estimation based on keystone transform [J]. IEEE transactions on signal processing, 2016, 64(15): 4013 - 4026. DOI: 10.1109/TSP.2016.2558161
- [6] HUANG P H, LIAO G S, YANG Z W, et al. Ground maneuvering target imaging and high-order motion parameter estimation based on second-order keystone and generalized hough-HAF transform [J]. IEEE transactions on geoscience and remote sensing, 2017, 55(1): 320 - 335. DOI: 10.1109/TGRS.2016.2606436
- [7] ZHU C Y, LI X P, SHI L, et al. A new fast Doppler shift and Doppler rate joint acquisition method for hypersonic vehicle communications [C]//Proceedings of International Symposium on Antennas and Propagation (ISAP). IEEE, 2018: 1 - 2
- [8] WAQAS A, LECHNER G, NGUYEN K, et al. Particle filter for joint carrier phase, Doppler shift and Doppler rate estimation and data detection [C]//Proceedings of IEEE Latin-American Conference on Communications (LATINCOM). IEEE, 2021: 1 - 6. DOI: 10.1109/LATINCOM53176.2021.9647810
- [9] LIU Y S, ZHANG S, GAO F F, et al. Uplink-aided high mobility downlink channel estimation over massive MIMO-OTFS system [J]. IEEE journal on selected areas in communications, 2020, 38(9): 1994 - 2009. DOI: 10.1109/JSAC.2020.3000884
- [10] DONG K Y, SHI J, WANG Z Y, et al. Performance analysis of orthogonal time frequency space modulation under time-varying Doppler channels [C]//The 34th Annual International Symposium on Personal, Indoor and Mobile Radio Communications (PIMRC). IEEE, 2023: 1 - 6. DOI: 10.1109/PIMRC56721.2023.10293809
- [11] SHAN Y R, WANG F G. Low-complexity and low-overhead receiver for OTFS via large-scale antenna array [J]. IEEE transactions on vehicular technology, 2021, 70(6): 5703 - 5718. DOI: 10.1109/TVT.2021.3072667
- [12] RAVITEJA P, PHAN K T, HONG Y, et al. Interference cancellation and iterative detection for orthogonal time frequency space modulation [J]. IEEE transactions on wireless communications, 2018, 17(10): 6501 - 6515. DOI: 10.1109/TWC.2018.2860011

Biographies

SHAN Yaru received her BE degree from the School of Electronic and Information Engineering, Beijing Information Science and Technology University, China in 2018. She is currently pursuing her PhD degree with the State Key Laboratory of Rail Traffic Control and Safety, Beijing Jiaotong University, China. Her current research interests include signal processing, orthogonal time frequency space, signal detection in high-speed scenarios, and integrated sensing and communication.

WANG Fanggang (fgwang@bjtu.edu.cn) received his BE and PhD degrees from the School of Information and Communication Engineering, Beijing University of Posts and Telecommunications, China in 2005 and 2010, respectively. He was a post-doctoral fellow with the Institute of Network Coding, The Chinese University of Hong Kong, China from 2010 to 2012. He was a visiting scholar with the Singapore University of Technology and Design in 2014, and with the Massachusetts Institute of Technology, USA from 2015 to 2016. He is currently a professor with the State Key Laboratory of Advanced Rail Autonomous Operation, Frontiers Science Center for Smart High-Speed Railway System, School of Electronics and Information Engineering, Beijing Jiaotong University, China. His research interests include wireless communications, signal processing, and information theory. He served as a technical program committee member for several conferences. He served as an editor for *IEEE Communications Letters*.

HAO Yaxing received his BE degree from the School of Electronic and Information Engineering, Beijing Jiaotong University, China in 2021, where he is currently pursuing his PhD degree with the State Key Laboratory of Rail Traffic Control and Safety. His current research interests include signal processing, orthogonal time frequency space, and signal detection in high-speed scenario.

HUA Jian received his MS degree from Harbin Engineering University, China, and now works at ZTE Corporation as an intermediate engineer. His research interests include phase noise model and compensation scheme design, waveform modulation and other technologies in terahertz communication scenarios.

XIN Yu graduated with a PhD degree from Beijing University of Posts and Telecommunications, China in 2003. He currently works at ZTE Corporation as a senior engineer and senior expert in technology pre-research, specializing in wireless communication technology. He first put forward the FB-OFDM and GFBOFDM waveform schemes and has published dozens of papers on waveform research. He is currently responsible for pre-research on candidate new waveforms for 6G.